

Cite this: DOI: 10.1039/c2sm25192b

www.rsc.org/softmatter

PAPER

Structural properties of the dipolar hard-sphere fluid at low temperatures and densities

Lorenzo Rovigatti,^{*a} John Russo^a and Francesco Sciortino^b

Received 25th January 2012, Accepted 4th April 2012

DOI: 10.1039/c2sm25192b

Through extensive state-of-the-art numerical simulations, we study the behavior of the dipolar hard sphere model at low temperatures and low densities, shedding light on a region of the phase diagram where a topological phase transition has long been thought to occur. We show that the system exhibits remarkable and unusual behaviors, like a very low density percolation locus and a stabilization of rings over chain structures. This unexpected abundance of rings comes from a delicate balance between the lower ring energy and the end-to-end chain entropy, and hints at a possible mechanism for the suppression of the gas–liquid phase separation. Our results open the possibility for refined theoretical approaches which, in addition to the previously encompassed chain and branched geometries, must also include the significant contribution arising from ring formation.

I. Introduction

The dipolar hard sphere (DHS) model is of paramount importance in the physics of disordered systems.^{1–5} It consists of a point dipole embedded in the center of a hard sphere, and it is the simplest model which incorporates anisotropic long-range interactions. Notwithstanding its simplicity, the DHS model is still the subject of thorough investigations, aimed in particular at understanding its low-temperature (T) and low-density (ρ) behaviour. From a theoretical point of view, the main difficulty arises from the fact that at low T and low ρ the phase behaviour of the model is determined by the competition between condensation and self-assembly. The condensation of dipolar particles, analogous to the usual gas–liquid phase transition, was first predicted by de Gennes and Pincus⁶ after observing that the spherically averaged interaction between dipoles is attractive. On the other hand, dipolar particles self-assemble into linear and branched structures with the dipoles aligned in the (energetically favorable) nose-to-tail geometry.^{2,7–10} The anisotropic aggregation of particles which results from the self-assembly process was long thought to be the mechanism responsible for the suppression of isotropic condensation and the absence of a phase transition between disordered states. This belief was completely reverted by theoretical studies¹¹ which showed that self-assembly alone is capable of sustaining a phase transition. Such a *topological phase transition* originates from the effective interactions between topological defects on the self-assembled dipolar chains. The topological defects relevant to the phase transition are the

chain ends, which provide an effective repulsion between the chains,¹¹ and the *Y-shaped* junctions, which instead provide an effective attraction. The essential properties of the topological phase transition can be studied both by mean-field theories¹¹ and thermodynamic perturbation theories,^{12,13} showing that criticality arises only if the ratio between the energy cost of junction formation over the energy cost of chain-end formation is within a specific range of values. Whether such an energy ratio in the DHS potential is consistent with the possibility of observing a topological phase transition is still unknown.

The low- T and low- ρ properties of the zero-field DHS model in three dimensions (3D) are not only hard to grasp from a theoretical point of view, but also pose significant challenges to both experimental and computational studies. From an experimental point of view, one is faced with the difficulty of generating single crystal magnetic cores of suitable size and without any residual isotropic attraction (which would artificially promote the condensation of the dipoles). From a computational point of view, the major challenges come from the expensive long range electrostatic calculations and from the long relaxation times of the structures (chains and networks) into which the dipoles self-assemble. Most of the simulation studies have thus been plagued by equilibration issues or severe finite size effects. These difficulties have inspired a lot of work studying model systems that are easier to solve numerically and that converge asymptotically on the DHS as a function of some parameter.^{3,14–16} Another line of research concentrated on the study of temperature-dependent valence models,^{12,13} successfully locating the topological phase transition, and finding very good agreement with the theoretical predictions.

Recently, we have reported¹⁷ a numerical study of the density fluctuations in the DHS, finding no evidence of the putative gas–liquid critical point in the region of densities and temperatures

^aDipartimento di Fisica, Università di Roma La Sapienza, Piazzale A. Moro 5, 00185 Roma, Italy. E-mail: lorenzo.rovigatti@uniroma1.it

^bDipartimento di Fisica and CNR–ISC, Università di Roma La Sapienza, Piazzale A. Moro 5, 00185 Roma, Italy

where the transition was predicted to occur.^{3,14–16,18} Even more interestingly, the reason for the absence of the topological phase transition in such a region was not related to the high energy cost of junction formation, as in one of the expected theoretical scenarios, but to the breakdown of the mean-field approximations at low T and low ρ . These results open up a new scenario for the DHS model, where new theoretical modeling is needed in order to explain its phase behaviour. In the present work we carefully study the structural properties of the DHS fluid at low T and low ρ , as a first step in this endeavour. We use highly efficient MC simulation techniques and extended computational resources to access, in equilibrium in the isothermal–isochoric ensemble, the unexplored T and ρ region where previous attempts had incorrectly predicted a gas–liquid coexistence. We provide detailed structural information as well as a study of the aggregate topologies to provide accurate data for refined theoretical modelling. In particular, we focus on chains and rings, which are the most common structures found in low- T , low- ρ DHS fluids.^{19,20} The interplay between these structures has been the center of numerous studies. Small-angle neutron scattering^{21–23} and TEM²⁴ experiments have shown that the structure factor at small wavelengths displays a power-law behaviour due to the aggregation of particles in finite-size and long-lived clusters. Many simulations and theoretical approaches were devoted to interpreting the structural signatures of low- T ferrofluids.^{25–30} Simulations in quasi two dimensions suggested that at very low T and ρ the system is mainly composed of isolated rings. Indeed, it has been theoretically shown that the ground state in the quasi-2D system is a single ideal ring³¹ for sizes larger than 4. As the density is increased, the average size of rings increases until they break into open chains³² due to entropic effects. As the density is further increased the chains start branching until they form a percolated network.¹⁹

We aim to generate information which can be used to provide appropriate parameters which can help to map the DHS model onto patchy particle models³³ that can be analytically solved within the Wertheim formalism.^{34,35} We find that the DHS model at low T exhibits remarkable and unusual behaviors, like a very low density percolation locus and a stabilization of rings over chains, resulting in a depletion of the number of chain ends. We speculate that this excess number of rings is a possible mechanism for suppressing the gas–liquid phase separation.

The paper is organized as follows. In Section II the model and the simulation methods are presented. Section III shows the results and Section IV contains a brief summary and a discussion of the results.

II. Methods

A. Model and computational details

The pair interaction potential between two dipolar hard spheres i and j is

$$u(i, j) = u_{HS}(r_{ij}) + \frac{\boldsymbol{\mu}_i \cdot \boldsymbol{\mu}_j - 3(\boldsymbol{\mu}_i \cdot \hat{\mathbf{r}}_{ij})(\boldsymbol{\mu}_j \cdot \hat{\mathbf{r}}_{ij})}{r_{ij}^3} \quad (1)$$

where \mathbf{r}_{ij} is the vector connecting the centers of particles i and j , $r_{ij} = |\mathbf{r}_{ij}|$, $u_{HS}(r_{ij})$ is the hard sphere potential and $\boldsymbol{\mu}_i$ is the dipole moment of particle i . In the following, the Boltzmann constant

$k_B = 1$, $\beta = 1/T$, lengths are measured in units of particle diameter σ and energy in units of μ^2/σ^3 . In these units, the most energetically favorable configuration is the nose-to-tail contact geometry, with an energy contribution of $u = -2$ (Fig. 1(a)). This absolute minimum is responsible for the characteristic chain-like structures which become prominent at low T . A relative minimum arises from the side-to-side antiparallel geometry, corresponding to a pair interaction energy of $u = -1$ (Fig. 1(b)).

The long range nature of the dipolar interaction and the clustering process hinders the possibility of carrying out equilibrium simulations in the low T ($T \lesssim 0.2$), low ρ region *via* conventional methods. Indeed, when thermal fluctuations become of the order of one tenth of the nose-to-tail energy, a significant chaining process starts to take place. In order to explore the low- T and low- ρ region in equilibrium we implement special Monte Carlo state-of-the-art moves and techniques specifically aimed at the DHS system.

One of the biggest difficulties in the simulation of self-assembly processes is the fact that the structures that are formed are located in a very small region of the phase space, and are thus difficult to sample. Moreover, once these structures are formed, the breaking of bonds becomes a rare event, which prevents the sampling of independent configurations. An efficient way to overcome these difficulties is to facilitate the formation and breakage of bonds *via* biased Monte Carlo moves.³⁶ In this work we adapt the aggregation-volume-bias (AVB) algorithm³⁷ which, given the definition of the region around each particle where bonds are stronger, accelerates both bond formation and bond breakage by moving particles into and out of these regions.

For the DHS model the most favourable bonding configurations correspond to the head–tail geometry, as shown in Fig. 1(a), and we thus define two virtual bonding regions (BR) on the poles of each particle. A bonding move consists in selecting the bonding region of a particle (say for example the north pole), and then moving the complementary pole (south pole) of another particle into this region. The reverse move consists instead in moving a particle out of the bonding region to a random location in the sample. Following the Kern–Frenkel idea,³⁸ the bonding regions are shaped as truncated cones (Fig. 1(c)) of angular width $\theta = 0.873 \text{ rad}$ ($\cos(\theta) = 0.64$) and range $\delta = 0.4 \sigma$. Two particles i and j are considered virtually bonded if their relative distance is

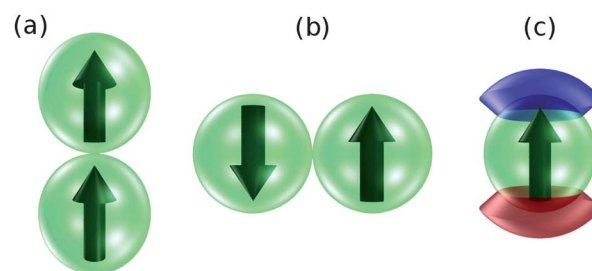


Fig. 1 (a) Nose-to-tail contact configuration corresponding to an absolute minimum in the interaction energy of $u = -2$ (in natural units). The arrows represent the point dipole embedded in the hard spheres. (b) Antiparallel contact configuration corresponding to a relative minimum of $u = -1$. (c) A single DHS with northern (blue) and southern (red) virtual bonding regions highlighted.

smaller than $\sigma + \delta$ and if $\mu_i \cdot \mu_j > \cos\theta$, corresponding to a volume $V_{AVB} = \frac{4}{3}\pi[(\sigma + \delta)^3 - \sigma^3] \frac{1 - \cos\theta}{2} = 1.3\sigma^3$. We define N_i as the number of particles which are in the BR of i . More precisely, two AVB moves are introduced:³⁷

1. With probability p_{AVB} we choose a random particle i and then we choose, randomly, another particle j which is in the BR of i . We move particle j out of the BR of particle i , inserting it with a random orientation. If no particles are found in the BR of i , the move is *a priori* rejected. We accept the move with probability

$$p_{in \rightarrow out} = \frac{1 - p_{AVB} N_i (4\pi V - V_{AVB})}{p_{AVB} (N - N_i) V_{AVB}} e^{-\beta\Delta U}$$

2. With probability $1 - p_{AVB}$ we choose a random particle i and a random particle j which is not inside the BR of i . We move particle j into the BR of particle i with a proper orientation to guarantee virtual bonding. We accept the move with probability

$$p_{out \rightarrow in} = \frac{p_{AVB} (N - N_i - 1) V_{AVB}}{1 - p_{AVB} (N_i + 1) (4\pi V - V_{AVB})} e^{-\beta\Delta U}$$

The value of p_{AVB} can be used to tune the relative acceptance probabilities for these two moves. A value of $p_{AVB} = 0.5$ was adopted throughout this work. We have thoroughly tested the AVB algorithm for models of associating particles where chaining and branching are dominant.^{12,13} We found that the AVB moves allow for equilibration down to temperatures $k_B T/u_b \approx 0.060$, where u_b is the typical bonding energy. This maps onto $T \approx 0.12$ for the DHS case, where $u_b \approx 2$. Note that the implemented AVB algorithm only acts on the process of forming and breaking chain structures. The process of breaking/forming branching points is equilibrated by standard Monte Carlo roto-translational moves, *i.e.* moves in which a random displacement and/or rotation is applied to each particle. Indeed, branched configurations are characterized by u_b values smaller than the nose-to-tail ones. This has been checked in the context of associating particle models^{12,13} the AVB algorithm does not result in any significant speed-up when also encoded for branching interactions. We fix a 1 : 1 frequency ratio between rotations/translations and biased moves. In the following, we define a MC step as N attempts to perform a rotation/translation or an AVB move (where N is the number of particles in the system). A measure of the efficiency of the AVB method will be provided in the following section, where the bond–bond autocorrelation function is reported.

Long range dipolar interactions are taken into account using Ewald sums with conducting boundary conditions.³⁶ In order to improve performance we used a mesh-based cubic spline interpolation for cosine and sine calculations, resulting in a $\sim 30\%$ speed-up. Such an approximation results in a precision in the energy evaluation of 10^{-6} .

We study a system composed of $N = 5000$ particles at six different densities ($\rho\sigma^3 = 0.007, 0.028, 0.056, 0.084, 0.114, 0.140$) and four different temperatures ($T = 0.125, 0.140, 0.155, 0.170$). For $T < 0.125$, equilibration times become prohibitive with present numerical resources. The lowest investigated T required 10 months of calculations on a Xeon 5050 core.

We note that the box sizes employed in the simulations (whose values range from 33 to 90, depending on the density) are about one order of magnitude larger than the average chain persistence length (see Section IIID). In addition, we check that the chains never percolate. Moreover, when a percolated network is present, the mesh size of its structure is always significantly smaller than the box length.

B. Bond definition and cluster classification

To quantify the connectivity properties of the system, a definition of a bond between a pair of particles is required. Given the continuous nature of the dipole–dipole interaction, bonding cannot be unambiguously defined. In the past, criteria based on cut-off distances^{3,19} or pair interaction energy thresholds^{3,4,25,27,39–41} have been proposed. Since sharp energy thresholds may lead to an underestimation of the branching, which is a key factor in topological phase transitions, and since the position r_b of the first minimum of the $g(r)$ is not very sensible on T or ρ (see Section 3.2), we combine the two approaches and define particles i and j as being bonded if $r_{ij} < r_b = 1.3$ and $u(i,j) < 0$. This criterion is somewhat similar to the “entropic” criterion proposed by Holm *et al.*,²⁷ with the difference being that the criterion employed here also takes into account the role of the branching due to anti-parallel geometry, which is not allowed by the former. Since this type of branching occurs only at intermediate ($\rho \geq 0.05$) densities, the two criteria are equivalent in the low- ρ limit.

To provide evidence that the length of our simulations is sufficient to probe equilibrium states, we evaluate the bond–bond autocorrelation function $C_b(\#_{MC})$. This quantity is defined as the probability that a bond existing at the beginning also exists after $\#_{MC}$ steps, quantifying how fast the network topology rearranges. Fig. 2 shows $C_b(\#_{MC})$ for three temperatures: $T = 0.125$, 0.155 and 0.170. It is interesting to observe that, at very low T , the system loses the memory of its initial state faster at higher ρ . This is consistent with the fact that, at low T , the lowest energy geometry is the one in which a particle is in the core of an isolated infinitely long chain. We also note that the shape of the correlation function can be properly modelled *via* a weakly stretched exponential (stretching parameter ≈ 0.9), reflecting the different local bonding geometries.

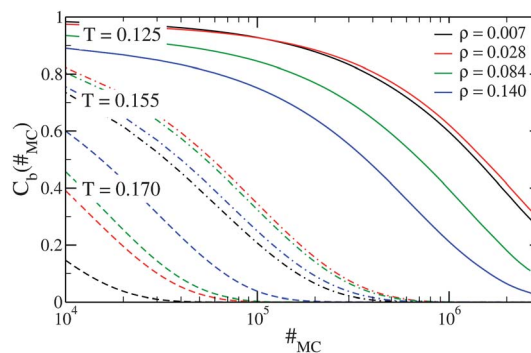


Fig. 2 Bond–bond autocorrelation function C_b as a function of the number of MC steps $\#_{MC}$ for four different densities and $T = 0.125$ (full lines), $T = 0.155$ (dashed-dotted lines) and $T = 0.170$ (dashed lines).

Employing the previous bonding criterion, we classify all clusters according to their bonding topologies in three groups: (i) **chains**: clusters containing two ends (*i.e.* particles with just one bonded neighbor) connected by particles with only two bonded neighbors; (ii) **rings**: clusters containing only particles with two bonded neighbors; (iii) **branched structures**: clusters containing at least one particle with more than two bonded neighbors.

III. Results

To provide a pictorial representation of the studied systems, Fig. 3 shows snapshots of equilibrium configurations of DHS systems at three different values of T and for the whole range of studied ρ . Two trends are already clearly distinguishable. First, as ρ increases, both chains and rings progressively merge together to form branched structures. Secondly, a decrease in T is accompanied with an increase in the number of rings, at the expense of the chain structures.

In the following we study in detail the structural properties at all these state points.

A. Potential energy

Fig. 4 shows the configurational potential energy per particle U as a function of ρ for all studied T . The energy shows a very weak ρ dependence, especially on lowering T , a clear signature of the onset of a self-assembly process.^{8,42} Indeed, self-assembly is characterized by the formation in the fluid phase of well defined structures (clusters), in which particles have a characteristic energy. When increasing density results only in an increase in the

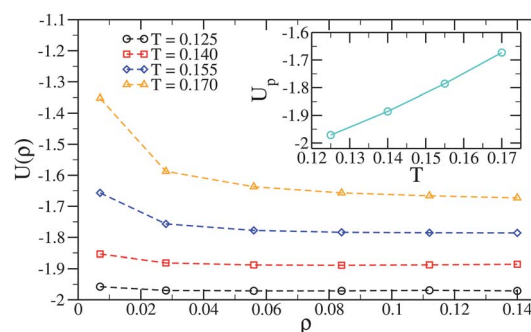


Fig. 4 Potential energy per particle $U(\rho)$ as a function of ρ for different T . Points are simulation results. Dashed lines are a guide for the eye. Inset: height of the plateau U_p for $T = 0.125, 0.140$ and 0.155 .

number of such structures, then the energy does not depend significantly on density.

To provide hints on the origin of the energy saturation with ρ , we examine the energy of clusters of different sizes. We first partition particles into clusters and separate them into three groups: chains, rings and branched structures, as discussed in section II B. As we will discuss in more detail in the following, at the lowest ρ most of the particles are in chains and rings. On increasing ρ , the number of particles in chains and rings drops in favor of extended branched structures, which percolate beyond a critical ρ . Here we focus primarily on chains and rings. The intra-cluster energy of chains and rings in the context of the DHS model has been previously addressed.¹⁹ An expression for the ground state energy per particle $e_c(s)$ in a chain of size s has been

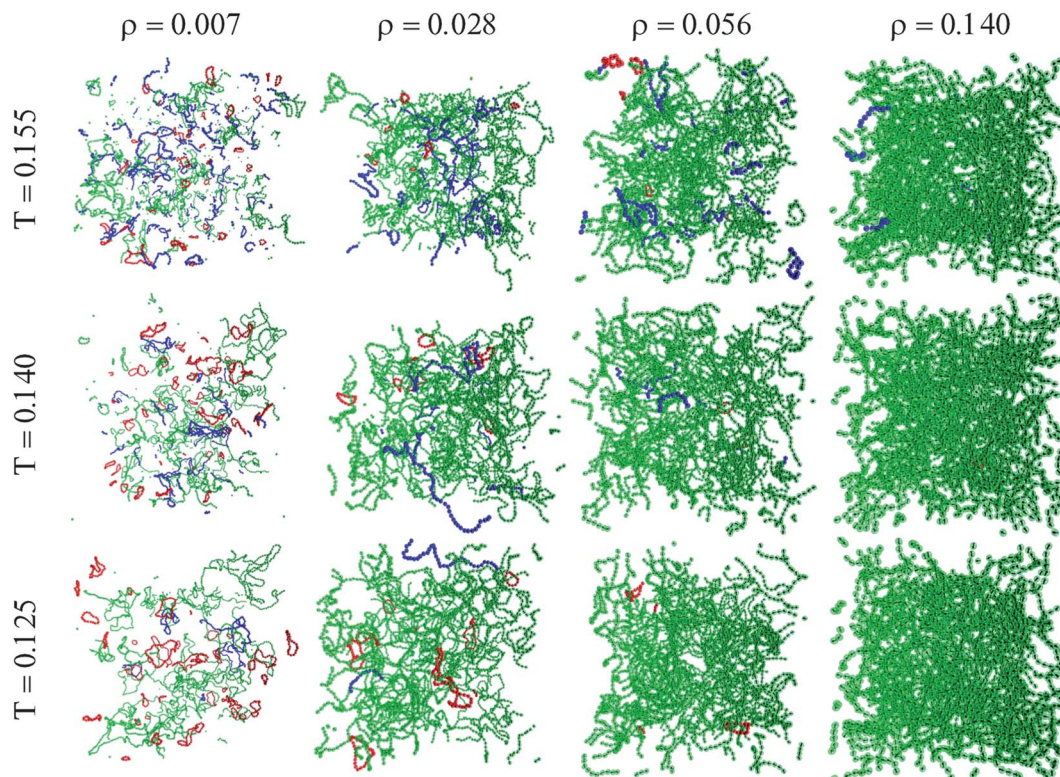


Fig. 3 Typical snapshots of equilibrium configurations of DHS at $T = 0.125, 0.140, 0.155$ and $\rho = 0.007, 0.028, 0.056, 0.140$. The different cluster topologies are depicted with different colors: chains (blue), rings (red) and branched structures (green).

proposed, based on the assumption that chaining produces a rescaling by a factor α (to take into account beyond-nearest neighbor interactions), of the dimer head-to-tail ground state energy $2\mu^2/\sigma^3$. According to this assumption, each bond contributes an energy $\alpha(2\mu^2/\sigma^3)$. Since there are $s - 1$ bonds in a chain, $e_c(s, T = 0) = \alpha(2\mu^2/\sigma^3) \frac{s-1}{s}$. This ground state expression has been generalized at finite T ¹⁹ by retaining the s dependence as:

$$e_c(s) = -e_0^c + \frac{e_1^c}{s}. \quad (2)$$

Here e_0^c is the bond energy for infinitely long chains and e_1^c accounts for finite size effects.

A similar approach can be applied to rings. Since the angle between the dipole moments of two nearest-neighbor particles in a ring of size s is $2\pi/s$, the ring energy at $T = 0$ can be written as $\alpha(2\mu^2/\sigma^3) \left[3 + \cos\left(\frac{2\pi}{s}\right) \right] / 4$, whose finite T generalization reads¹⁹

$$e_r(s) = -e_0^r + \frac{e_1^r}{s^2}. \quad (3)$$

All the coefficients, namely e_0^c , e_0^r , e_1^c , and e_1^r , are expected to depend only on T .

Fig. 5 shows $e_r(s)$ and $e_c(s)$ as functions of the cluster size for a system at $T = 0.125$ and $\rho = 0.007$, and the corresponding fit according to eqn (2) and 3. The fit properly represents the s dependence of the particle energy. The asymptotic value e_0^c , representing the average bond energy in large chains, is reached only when $s \geq 100$. The asymptotic value e_0^r , referring to rings, is instead reached when $s \geq 50$, as expected on the basis of the s^{-2} dependence in $e_r(s)$. e_0^c and e_0^r are almost ρ independent and the fit provides the same value e_0 within statistical error. The T dependence of e_0 is presented in the inset of Fig. 5. e_0 decreases with T , possibly due to the reduced vibrational contribution to the potential energy. To confirm the vibrational nature of the T dependence of e_0 we evaluate the inherent structures (IS),^{43,44} by

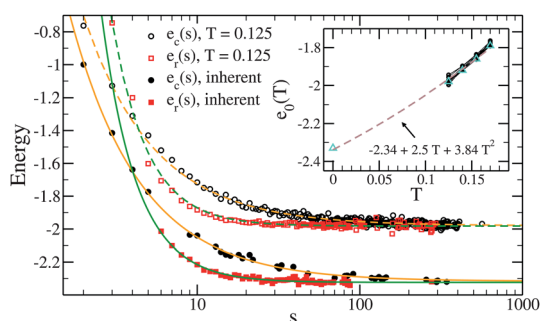


Fig. 5 Potential energy of particles in chains (open circles) and rings (open squares) of size s at $\rho = 0.007$ and $T = 0.125$ and for the inherent structure (full symbols). Lines are fit to the simulation data according to eqn (2) (orange dashed and full lines) and (3) (green dashed and full lines). Inset: e_0 at $\rho = 0.007$ for all studied T and for the inherent structure (triangles). To provide evidence of the ρ independence of e_0 we also show the corresponding value for all investigated densities (small black circles). The brown curve is a quadratic fit to the triangle points in which the harmonic linear term $2.5T$ has been fixed.

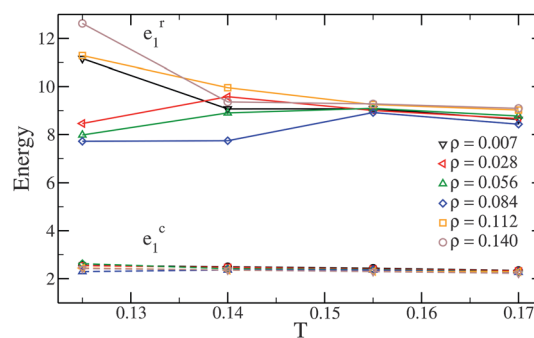


Fig. 6 Fit parameters e_1^c (dashed lines) and e_1^r (full lines) for all the state points.

minimizing the energy of a set of equilibrium configurations at $\rho = 0.007$ and $T = 0.125$. The functional form describing the s dependence of the chains and rings remains identical. The average bond energy in the IS configuration is -2.33 , to be compared to the value of the energy per particle in the *close-packed* anti-ferromagnetic configuration, equal to -2.56 .⁶ The inset also shows that the T dependence of e_0 , including the $T = 0$ inherent structure value, can be modelled assuming a weak anharmonicity as $e_0(T) = -2.34 + 2.5 k_B T + 3.84(k_B T)^2$.

The best-fit values of the remaining fitting parameters (e_1^c and e_1^r) are shown in Fig. 6. Such values are very similar to the ones found in quasi-2D DHS.¹⁹

B. $g(r)$ and $S(q)$

To quantify the structural changes of the DHS fluid at different T and ρ , we compute the radial distribution function $g(r)$. The $g(r)$ provides information on the relative distance between particles in the system. Fig. 7(a) shows the T effect on $g(r)$ at densities

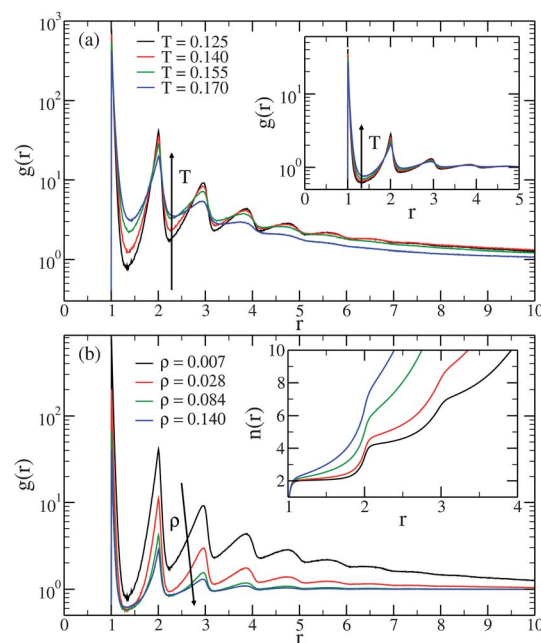


Fig. 7 (a) $g(r)$ for all the studied temperatures at $\rho = 0.007$ (main panel) and $\rho = 0.140$ (inset). (b) $g(r)$ at fixed $T = 0.125$ for different densities. Inset: average number of neighbors $n(r)$ for the same state points.

$\rho = 0.007$ and $\rho = 0.140$ (inset). The $g(r)$ is well structured even at the highest investigated T . Upon lowering T , the minima deepen and the height and sharpness of the peaks increase. At large r , $g(r)$ approaches one from above, reflecting the presence of spacial inhomogeneities, intrinsic to the cluster structure of the system. Similarly, the radial positions of the third and following peaks increase. The first two phenomena highlight the increasing bond localization which takes place in this T region.¹⁷ The shift of the secondary peaks towards values of r which are multiples of σ suggests that chains become straighter on cooling, or, in other words, the persistence length of the chains increases. It is interesting to observe that the first peak becomes more and more resolved on cooling, and that the amplitude of the first minimum approaches zero. Under these conditions, the definition of nearest neighbour in terms of the relative distance becomes precise.

At higher ρ (inset of Fig. 7(a)), the system always contains a percolating structure (see Section III C) and the $g(r)$ becomes more similar to the one observed in simple fluids. Now at large r , $g(r)$ oscillates around one with a periodicity σ . The shape of the peaks is still asymmetric, reflecting the preferential one-dimensional growth of the equilibrium aggregates.

In order to clarify the effect of ρ on the structure, we study the number of neighbors $n(r)$ within a sphere of radius r centered on an arbitrary particle, defined as

$$n(r) = 4\pi\rho \int_0^r r'^2 g(r') dr'. \quad (4)$$

The result is shown in the inset of Fig. 7(b) for $T = 0.125$. For low and intermediate ρ , a plateau develops for $1 < r < 2$ in which $n(r) \approx 2$, clear evidence that, locally, particles are coordinated with only two neighbors, *i.e.* that the system associates mostly in chains and rings. At high ρ , the number of neighbors in the first shell increases, signaling the presence of branching and the formation of more complex structures.

The large value of the low q limit of the structure factor $S(q)$, calculated as $S(q) = \frac{1}{N} \left\langle \sum_{i=1}^N \sum_{j=1}^N e^{iq \cdot (r_i - r_j)} \right\rangle$ and presented in Fig. 8, provides another sign of the strong association occurring in the system. Indeed, in a system of independent (ideal gas) clusters, $S(q)$ reflects the properly averaged cluster form factor

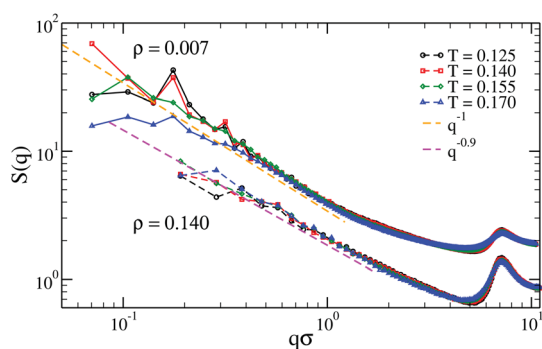


Fig. 8 $S(q)$ for all the studied temperatures at $\rho = 0.007$ (full lines) and $\rho = 0.140$ (dashed lines). The $\rho = 0.007$ data has been shifted upwards by adding 1. Dashed lines are power-law curves with exponents -1 (orange) and -0.9 (magenta).

and it approaches the second moment of the mean cluster size when $q \rightarrow 0$. The most visible T effect can be found in the shape of the first peak, which becomes more and more asymmetric upon lowering T .⁴⁵ At larger ρ , interference between different clusters (which are now connected in a percolating network), significantly lowers the small- q value of $S(q)$. Interestingly, no significant T dependence is observed, suggesting that the system has reached its final structure and only minor changes take place. Such a property is characteristic of equilibrium gels.^{45,46} The only effect of decreasing T is visible in the small increase in the height and asymmetry of the first peak.

$S(q)$ shows a clear change of “scaling” behaviors in different q -windows. The low- q behavior of the structure factor can often be related to the fractal dimension D of the aggregates *via* $S(q) \propto (q\sigma)^{-D}$. As Fig. 8 shows, the region where a power-law behavior is clearly and unambiguously observed is less than one decade. Under these conditions, it is extremely hard and possibly misleading to extract exponents. A slope of order one, consistent with a strong signature from chains, is consistent with the scaling at small q in the region $0.3 \lesssim q \lesssim 1$.³⁰

C. Connectivity properties and degree of polymerization

We now explore the global connectivity properties of the DHS model. In particular, we evaluate the percolation locus, separating percolating and non-percolating state points. Percolation (*via* physical interactions) is a pre-requisite for the onset of a second-order critical phenomenon.⁴⁷ Indeed, both in spherically interacting potentials,⁴⁸ as well as in limited-valence patchy interactions,⁴⁹ on cooling the percolation line is always encountered before the gas–liquid instability line. We define a state point as percolating if more than half of its configurations contain a spanning cluster, *i.e.* a cluster which is connected to itself *via* periodic boundary conditions. The results of this analysis are summarized in Fig. 9. The percolation threshold extends to very low ρ (as low as $\rho \approx 0.01$ for the lowest studied T in equilibrium). This result once more suggests that the system is composed of rather long chains connected *via* branching points.

Another interesting observable in the study of the self-assembly process is the so-called degree of polymerization Φ , commonly defined in self-assembly studies as the fraction of

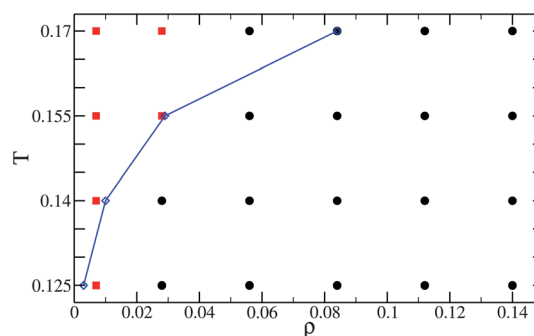


Fig. 9 Percolating (black circles) and non percolating (red squares) state points. The percolation line passes near the $T = 0.125$, $\rho = 0.007$ state point, which has almost half of the configurations ($\sim 49\%$) containing a spanning cluster. The blue symbols are the state points where the degree of polymerization is $\Phi \approx 0.99$.

particles associated into clusters^{50,51} ($1 - \Phi$ is conversely the fraction of particles in monomers). In the T - ρ window explored in the present study, the degree of polymerization is always very close to one (we find that $\Phi > 0.95$ for every studied state point but $T = 0.170$, $\rho = 0.007$). To provide a reference for further study we report in Fig. 9 the locus $\Phi = 0.99$.

D. Chains and rings

In this section we investigate the properties of chains and rings at low ρ ($\rho = 0.007$). We aim at providing accurate quantitative data on the structure of these clusters in the limit in which excluded volume cluster-cluster interactions are limited and the system can be, to a first approximation, considered as a mixture of polydisperse non-interacting clusters.

The fraction of particles involved in chains, rings and other branched structures at $\rho = 0.007$ and $\rho = 0.028$ is shown in Fig. 10. As shown in the figure, upon lowering T at fixed ρ , the fraction of particles in chains diminishes and the majority of the particles belong to large branched structures. On further cooling, these particles would give rise to a percolating structure, despite the small average ρ . The decrease in the number of particles in chains on cooling has thus a double origin. On one hand, the rings become more stable than chains (at comparable size) and indeed the number of particles in rings increases on cooling, and on the other hand, chains become longer and hence have a larger probability of branching. Despite this competing effect, even at the lowest T a significant fraction of particles is still in chains and rings. This allows us to carry out an analysis of the properties of such structures, similar to what has been done in the past in the investigation of equilibrium polymerization, in which ring formation is allowed.^{52,53} It is interesting to observe that the condition $n_r(T_x) = n_c(T_x)$ implicitly defines a cross-over

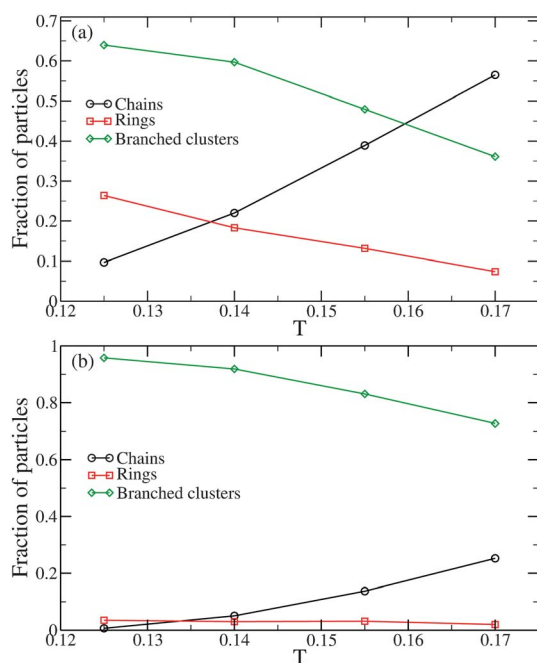


Fig. 10 Fraction of particles in chains (circles), rings (squares) and branched structures (diamonds) for all studied temperatures at (a) $\rho = 0.007$ and (b) $\rho = 0.028$.

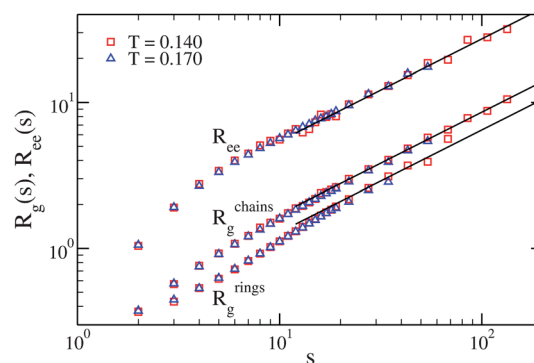


Fig. 11 Radius of gyration $R_g(s)$ of rings $R_g^{\text{rings}}(s)$ and chains $R_g^{\text{chains}}(s)$ and mean end-to-end distance $R_{cc}(s)$ of chains at $\rho = 0.007$ for $T = 0.140$ and $T = 0.170$. Lines through the $T = 0.140$ data are power laws with exponent 0.7.

temperature T_x , below which rings start to play a significant role. In the studied ρ -window we find $0.125 \leq T_x \leq 0.14$, a value within the range of temperatures previously estimated in quasi two-dimensional simulations.³¹

We start by calculating the radius of gyration $R_g(s)$ of rings and chains of size s (Fig. 11). In the scaling limit, *i.e.* for large s ,

$$R_g(s) = b \cdot s^\nu, \quad (5)$$

where the prefactor b is model (and, in principle, T) dependent, while the exponent $\nu = 0.5$ for a random walk and $\nu = 0.588$ in the case of a self-avoiding random walk (SAW).⁵⁴ $R_g(s)$ appears to be rather insensitive to T . Indeed, both the chain and ring radii of gyration do not display any significant change upon lowering T . In the limit of large s , *i.e.* $s > 20$, for both chains and rings a power-law dependence (eqn (5)) sets in, but with an exponent $\nu \approx 0.7$ significantly larger than the one expected for a SAW chain. While we cannot exclude the possibility that we are observing an intermediate cross-over region, the difference with the SAW exponent is significantly large to question if dipolar charged chains and rings belong to a different universality class. Indeed, in a previous study on the Stockmayer fluid⁵⁰ (*i.e.* in which the hard-sphere potential is replaced by a Lennard-Jones one) a similar value of ν was observed. The average end-to-end distance of chains, $R_{cc}(s)$, is also shown in Fig. 11. Like $R_g(s)$, $R_{cc}(s)$ is rather T independent and scales, within numerical uncertainty, with the same exponent $\nu \approx 0.7$.

To further characterize the chain geometry, we evaluate the angular correlation $\langle \cos(\theta) \rangle(n)$, where $\cos(\theta) = \hat{\mu}_i \cdot \hat{\mu}_j$, i and j are two particles belonging to the same chain, n is the “chemical” distance between them (*i.e.* the number of bonds separating the two particles) and angular brackets indicate an average taken over all pairs of particles (in the same chain) which are separated by n . We compare its behavior with the expected functional form

$$\langle \cos(\theta) \rangle(n) = \exp\left(-\frac{n}{l_p}\right) \quad (6)$$

where l_p is the chain persistence length. Fig. 12(a) shows both $\langle \cos(\theta) \rangle(n)$ and the best fits to eqn (6). Table 1 reports l_p for all studied T . Unlike b in eqn (5), lowering T from $T = 0.170$ to $T = 0.125$ results in a $\sim 100\%$ increase in l_p .

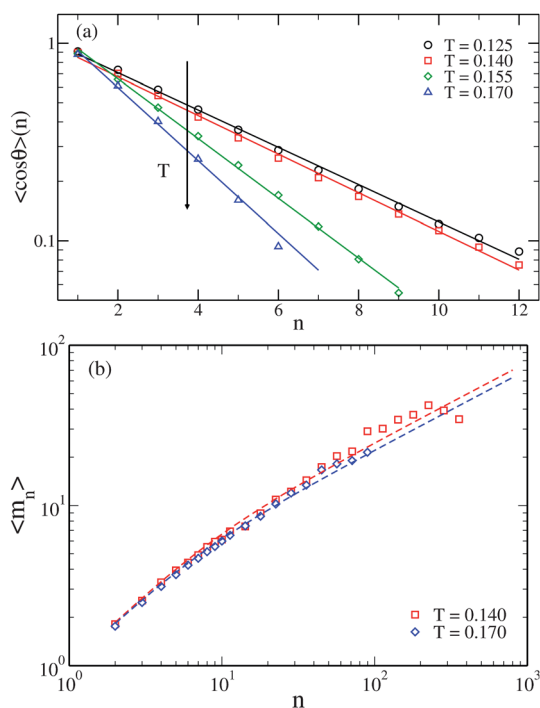


Fig. 12 (a) Average angular correlation $\langle \cos\theta \rangle(n)$ between particles as a function of the chemical distance n along the chain (symbols). Lines are exponential fits to eqn (6) restricted to small n . (b) Eqn (7) (dashed lines) and simulation results (symbols) for the mean squared magnetic moment $\langle m_n \rangle$ as a function of the chain length n for two different T .

Table 1 Average chain length \bar{l} , persistence length l_p and asymptotic mean internal energy per particle in chains and rings e_0 at $\rho = 0.007$ for all the studied temperatures

T	\bar{l}	l_p	e_0
0.125	64.2	4.6	-1.98
0.140	37.9	4.44	-1.92
0.155	15.2	2.87	-1.86
0.170	7.25	2.35	-1.79

To conclude, we analyze the mean squared magnetic moment of chains of size n , $\langle m_n \rangle$. Mendelev and Ivanov have provided a parameter-free expression for $\langle m_n \rangle$ in the dilute limit⁵⁵

$$\langle m_n \rangle = \sqrt{n + 2 \frac{K}{(1-K)^2} (n-1 + K^n - nK)} \quad (7)$$

where $K = \coth(\beta/2) - 2/\beta$. Fig. 12(b) shows simulation results and predictions from eqn (7) for $\langle m_n \rangle$ for two different values of T and $\rho = 0.007$. The theoretical predictions are in rather good agreement with the numerical results.

Next we focus on the chain distribution $n_c(s)$, the number of chains of size s . We showed elsewhere that for $s \geq 20$, $n_c(s) \sim \exp(-s/\bar{l})$.¹⁷ Fig. 13(a) shows the first moment of the distribution, the average chain length \bar{l} for all studied state points. Interestingly, at high T , \bar{l} shows a non-monotonic dependence as a function of ρ . This is in stark contrast to what is expected from an equilibrium polymerization process, in which only chaining is present. In the mean field, \bar{l} is predicted to scale as $\bar{l} \sim \rho^{1/2}$.⁵⁶ The

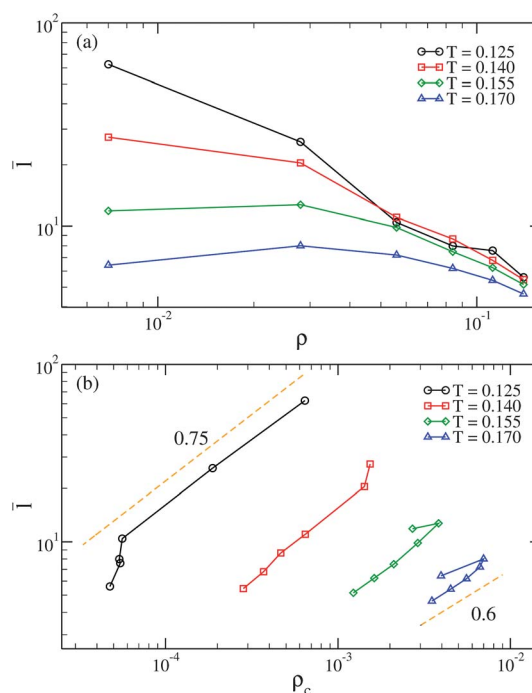


Fig. 13 (a) Log-log plot of the average chain length \bar{l} as a function of ρ for all the studied temperatures. (b) Same data but plotted as a function of the rescaled density N_c/V , where N_c is the number of particles in chains.

presence of a maximum stems from the equilibrium transformation of chains into branched structures. Indeed, within a mean-field description, the density of chains (ρ_c) increases with the density of chain ends (ρ_e) and decreases proportionally to the density of junctions (ρ_j), thus $\rho_c = k_1 \rho_e - k_2 \rho_j$, where k_1 and k_2 are proportionality factors and $\bar{l} \sim \rho_c^{-1}$. The corresponding scaling of ends and junctions is:¹¹ $\rho_e \sim \rho^{1/2} e^{-\varepsilon_e/T}$, and $\rho_j \sim \rho^{3/2} e^{-\varepsilon_j/T}$, where ε_e and ε_j are the energy costs of ends and junctions, respectively. By taking the derivative of the expression of the density of chains with respect to ρ , a minimum in ρ_c appears, resulting in a maximum for \bar{l} at $\rho^* \sim e^{-(\varepsilon_e - \varepsilon_j)/T}$. Note that $\varepsilon_e - \varepsilon_j$ is the energy released when a chain end bonds to form a junction, suggesting indeed that the density maximum is related to the assembly of the chains in branched networks.

Fig. 13(b) shows the same \bar{l} values but as a function of the reduced number density of particles in chains, ρ_c . In this representation, the internal equilibrium within the chain sub-system is considered, and \bar{l} returns to be a growing function of ρ_c , even if only in a finite interval. In this window, the ρ_c dependence of \bar{l} is consistent with a power law behavior, but with a T -dependent exponent between 0.6 and 0.75. As recalled before, in linear polymerization, mean-field approaches predict in the low- T , low- ρ region an exponent of 0.5.^{51,56,57} More accurate approaches predict, for dilute systems, 0.46 ± 0.01 .⁵⁶

The ring cluster size distribution $n_r(s)$ is shown in Fig. 14(a). The number of rings grows significantly on cooling, favored by the additional energetic stability of rings, as compared to chains of equal length, provided by the additional bond. It has been suggested, on the basis of a Flory-Huggins-type mean-field approximation,⁵² that $n_r(s)$ can be represented as

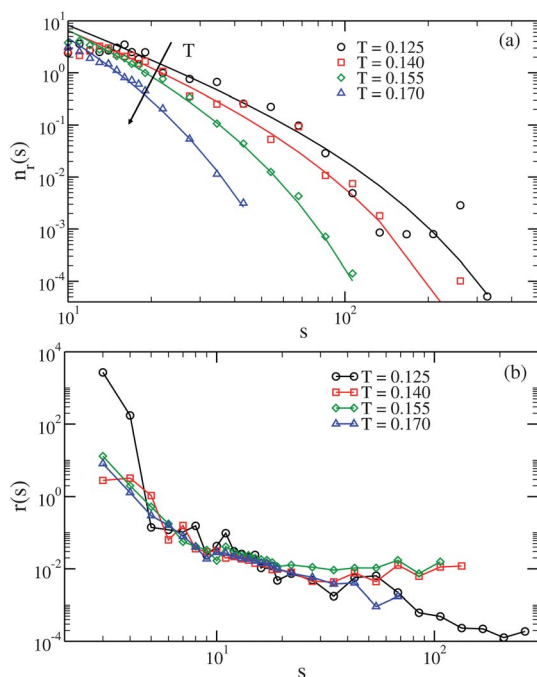


Fig. 14 (a) Number of rings $n_r(s)$ of size $s \geq 10$ at $\rho = 0.007$ for every studied temperature (symbols). Lines are best fits to eqn (8) limited to the region $s > 12$, with \bar{l} taken from Table 1. Imposing h to be equal for all T results in a value of $h = 2$, leaving only the amplitude c as a free, T dependent parameter. (b) $r(s)$ (see eqn (9) for definition) for all studied T at $\rho = 0.007$. $\Delta E(s)$ is computed *via* the calculated $e_r(s)$ and $e_c(s)$ values for $s < 10$ and *via* the associated fit functions (see Section III A) otherwise.

$$n_r(s) = c \exp\left(-\frac{s}{\bar{l}}\right) s^{-h} \quad (8)$$

where c is a normalization constant and h is a characteristic, T independent exponent. As shown in Fig. 14(a), imposing the known \bar{l} value, it is possible to properly model $n_r(s)$ (for $s \geq 15$) following eqn (8).

By definition, the ratio between $n_c(s)$ and $n_r(s)$ is equal to the ratio of the respective partition functions. Three elements contribute to controlling this ratio: (i) the different free energy contributions which arise from the different number of bonds in chains and rings of equal size. Assuming that at low T the dominant contribution is energetic, we expect that the ratio will depend on $e^{-\beta\Delta E(s)}$, where $\Delta E(s) \equiv s(e_r(s) - e_c(s))$ is the energy difference between a ring and a chain of equal size s ; (ii) the number of distinct modes which convert a ring to a chain, equal to the total number of bonds in the ring, s ; (iii) the different entropy of a chain compared to a ring, which can be approximated by the volume explored by the chain ends, $R_{ee}^3(s)$.

Fig. 14(b) shows the ratio,

$$r(s) \equiv \frac{n_r(s)}{n_c(s)} s R_{ee}^3(s) e^{-\beta\Delta E(s)} \quad (9)$$

for all the studied T . Apart from deviation at very small and very large s values, associated with the significant numerical noise under these extreme conditions, all the curves collapse on a single master curve for small and intermediate s . Even if the large s behavior is plagued by numerical uncertainties arising from the

small number of aggregates with such a large size, it appears plausible that $r(s)$ has a weak (or even no) dependence on s for large s , in agreement with previous results derived for equilibrium polymerization.⁵² We also note that eqn (9) is consistent with eqn (8), since it predicts that the ring distribution function is the product of the chain distribution function (and hence of an exponential function decaying with \bar{l}) times a power law in s , which accounts for the asymptotic behavior of the end-to-end cube distance, the linear s dependence as well as any residual s dependence in the bond energy, which has not yet reached its asymptotic value (see Fig. 5).

IV. Conclusions

The present study reports an in-depth characterization of the structural properties of DHS for $0.125 \leq T \leq 0.17$ and $0.007 \leq \rho \leq 0.14$, a window of T and ρ which, despite its relevance, was never explored before in simulation studies. To investigate such a region we have introduced specialized Monte Carlo biased moves, which favor the breaking and reforming of bonds, allowing us to effectively sample low- T and low- ρ configurations in equilibrium. Our results provide several hints on why no evidence of the phase transition, which was long thought to be hidden in this region, was recently found.¹⁷

Indeed, the theoretical approaches developed to predict the low T DHS behavior focused on the competition between bonding and chaining as the basic elements which control the thermodynamics of the system.¹¹ A new element brought in by the present study is the presence, in addition to chains and branched structures, of ring-shaped clusters. We have found that, at low T and ρ , rings become more probable than chains, since the additional energy gain of forming the additional bond which converts a chain into a ring compensates for the entropic loss associated with exploration of the volume available to the chain ends.

The dominance of rings over chains could affect the gas–liquid phase separation. Rings in fact have a negligible net magnetic moment and are thus weakly interacting objects. More importantly, they deprive the fluid phase of chain ends, which were predicted to sustain the topological phase separation.¹¹ In general, an energy-driven phase-transition relies on the energy gain of the fluid to form aggregates to overcome the entropy penalty of condensation. With rings being the majority cluster at low- ρ , there is virtually no energy gain in the transformation of the gas of rings into a branched liquid-like network. This can also be seen by considering the surface tension of the aggregates, which, at low- T (where entropy plays a minor role), is proportional to the energy difference between particles on the surface of the aggregate and particles inside the aggregate. The loss of chain ends due to ring formation lowers the surface tension of the fluid phase to a value close to zero, potentially suppressing the driving force to condensation.

Of course, a phase transition is still an open possibility for values of T lower than the ones we have investigated. In this case, the results of our study can be used to guide future theoretical modeling in the search of a mechanism which could sustain criticality. If the phase transition between a liquid and a gas indeed exists at lower temperatures than the one we have been able to explore,¹⁷ the gas phase should be modelled as a phase

rich in rings and not as a phase rich in chain ends, as has been assumed until now.

As an example of such modeling, the mapping of the DHS properties onto a patchy particle model appears to be a promising route,³³ especially if the model can be extended to incorporate the chain–ring equilibrium. In principle, it is possible to envision an asymmetric patchy particle model³³ in which the bond angle is comparable to the one characteristic of DHS (*i.e.* which give rises to similar $R_{ee}(s)$ and $\langle \cos(\theta) \rangle(n)$ to the one reported in Fig. 11 and 12) and in which the relative weight of rings and chains is controlled by the same ratio as the one discussed in eqn (9). Such a model, if properly benchmarked against the data reported in this article, could perhaps shed some light on the phase behavior of very low- T DHS systems.

Acknowledgements

We acknowledge support from ERC-226207-PATCHYCOLLOIDS and ITN-234810-COMPLOIDS. We thank P. J. Camp, S. Kumar, F. Romano, J. M. Tavares, P.I.C. Teixeira and M. M. Telo da Gama for relevant discussions.

References

- J.-M. Caillol and J. Chem. Phys., 1993, **98**, 9835.
- P. I. C. Teixeira, J. M. Tavares and M. M. Telo da Gama, *J. Phys.: Condens. Matter*, 2000, **12**, 411.
- G. Ganzenmüller, G. N. Patey and P. J. Camp, *Mol. Phys.*, 2009, **107**, 403.
- J. J. Weis and D. Levesque, *Phys. Rev. Lett.*, 1993, **71**, 2729.
- M. E. van Leeuwen and B. Smit, *Phys. Rev. Lett.*, 1993, **71**, 3991.
- P. G. de Gennes and P. A. Pincus, *Eur. Phys. J. B*, 1970, **11**, 189.
- R. van Roij, *Phys. Rev. Lett.*, 1996, **76**, 3348.
- R. P. Sear, *Phys. Rev. Lett.*, 1996, **76**, 2310.
- J. Dudowicz, K. F. Freed and J. F. Douglas, *J. Chem. Phys.*, 2003, **119**, 12645.
- J. Dudowicz, K. F. Freed and J. F. Douglas, *Phys. Rev. Lett.*, 2004, **92**, 045502.
- T. Tlusty and S. A. Safran, *Science*, 2000, **290**, 1328.
- J. Russo, J. M. Tavares, P. I. C. Teixeira, M. M. Telo da Gama and F. Sciortino, *Phys. Rev. Lett.*, 2011, **106**, 085703.
- J. Russo, J. Tavares, P. Teixeira, M. da Gama and F. Sciortino, *J. Chem. Phys.*, 2011, **135**, 034501.
- J. C. Shelley, G. N. Patey, D. Levesque and J. J. Weis, *Phys. Rev. E*, 1999, **59**, 3065.
- N. G. Almarza, E. Lomba, C. Martín and A. Gallardo, *J. Chem. Phys.*, 2008, **129**, 234504.
- G. Ganzenmüller and P. J. Camp, *J. Chem. Phys.*, 2007, **126**, 191104.
- L. Rovigatti, J. Russo and F. Sciortino, *Phys. Rev. Lett.*, 2011, **107**, 237801.
- Y. V. Kalyuzhnyi, I. A. Protsykevych and P. T. Cummings, *Europhys. Lett.*, 2007, **80**, 56002.
- J. M. Tavares, J. J. Weis and M. M. Telo da Gama, *Phys. Rev. E*, 2002, **65**, 061201.
- X. Chen, M. Yu-Qiang, H. Pak-Ming and T. Fu-Qiang, *Chin. Phys. Lett.*, 2005, **22**, 485.
- F. Kun, W. Wen, K. Pál and K. Tu, *Physical Review E*, 2001, **64**, 061503.
- M. Klokkenburg, B. Erné, A. Wiedenmann, A. Petukhov and A. Philipse, *Phys. Rev. E*, 2007, **75**, 051408.
- A. Wiedenmann, U. Keiderling, M. Meissner, D. Wallacher, R. Gähler, R. P. May, S. Prévost, M. Klokkenburg, B. H. Erné and J. Kohlbrecher, *Phys. Rev. B*, 2008, **77**, 184417.
- M. Klokkenburg, R. P. A. Dullens, W. K. Kegel, B. H. Erné and A. P. Philipse, *Phys. Rev. Lett.*, 2006, **96**, 037203.
- A. O. Ivanov, Z. Wang and C. Holm, *Phys. Rev. E*, 2004, **69**, 031206.
- J. Cerdà, E. Elfimova, V. Ballenegger, E. Krutikova, A. Ivanov and C. Holm, *Phys. Rev. E*, 2010, **81**, 011501.
- C. Holm, A. Ivanov, S. Kantorovich, E. Pyanzina and E. Reznikov, *J. Phys.: Condens. Matter*, 2006, **18**, S2737.
- S. Kantorovich, J. Cerdà and C. Holm, *Phys. Chem. Chem. Phys.*, 2008, **10**, 1883.
- E. Pyanzina, S. Kantorovich, J. Cerdà, A. Ivanov and C. Holm, *Mol. Phys.*, 2009, **107**, 571.
- P. J. Camp and G. N. Patey, *Phys. Rev. E*, 2000, **62**, 5403.
- T. Prokopenko, V. Danilov, S. Kantorovich and C. Holm, *Physical Review E*, 2009, **80**, 031404.
- H. Morimoto, T. Maekawa and Y. Matsumoto, *Phys. Rev. E*, 2003, **68**, 061505.
- J. Tavares and P. Teixeira, *Mol. Phys.*, 2011, **109**, 1077.
- M. Wertheim, *J. Stat. Phys.*, 1984, **35**, 19–35.
- M. Wertheim, *J. Stat. Phys.*, 1986, **42**, 459–477.
- B. Smit and D. Frenkel, *Understanding molecular simulations*, Academic, New York, 1996.
- B. Chen and J. I. Siepmann, *J. Phys. Chem. B*, 2001, **105**, 11275.
- N. Kern and D. Frenkel, *J. Chem. Phys.*, 2003, **118**, 9882.
- D. Levesque and J. J. Weis, *Phys. Rev. E*, 1994, **49**, 5131.
- J. M. Tavares, J. J. Weis and M. M. Telo da Gama, *Phys. Rev. E*, 1999, **59**, 4388.
- Z. Wang, C. Holm and H. W. Müller, *J. Chem. Phys.*, 2003, **119**, 379.
- R. Jones, *Soft Condensed Matter*, Oxford University Press, 2002.
- F. H. Stillinger and T. A. Weber, *J. Phys. Chem.*, 1983, **87**, 2833.
- F. Sciortino, *Journal of Statistical Mechanics: Theory and Experiment*, 2005, **5**, 15.
- J. Russo, P. Tartaglia and F. Sciortino, *J. Chem. Phys.*, 2009, **131**, 014504.
- E. Zaccarelli, I. Saika-Voivod, S. V. Buldyrev, A. J. Moreno, P. Tartaglia and F. Sciortino, *J. Chem. Phys.*, 2006, **124**, 124908.
- A. Coniglio and W. Klein, *J. Phys. A*, 1980, **13**, 2775.
- S. H. Chen, J. Rouch, F. Sciortino and P. Tartaglia, *J. Phys.: Condens. Matter*, 1994, **6**, 10855.
- E. Bianchi, P. Tartaglia, E. La Nave and F. Sciortino, *J. Phys. Chem. B*, 2007, **111**, 11765.
- V. Workum and J. F. Douglas, *Phys. Rev. E*, 2005, **71**, 031502.
- F. Sciortino, E. Bianchi, J. F. Douglas and P. Tartaglia, *J. Chem. Phys.*, 2007, **126**, 4903.
- J. P. Wittmer, P. van der Schoot, A. Milchev and J. L. Barrat, *J. Chem. Phys.*, 2000, **113**, 6992.
- A. Milchev, J. P. Wittmer and D. P. Landau, *Phys. Rev. E*, 2000, **61**, 2959.
- P.-G. De Gennes, *Scaling Concepts in Polymer Physics*, 1st edn, Cornell University Press, 1980, ISBN 080141203X.
- V. S. Mendelev and A. O. Ivanov, *Phys. Rev. E*, 2004, **70**, 051502.
- J. P. Wittmer, A. Milchev and M. E. Cates, *J. Chem. Phys.*, 1998, **109**, 834.
- Y. Rouault and A. Milchev, *Phys. Rev. E*, 1995, **51**, 5905.